Anisotropic carrier dynamics in a laser-excited Fe₁/(MgO)₃(001) heterostructure from real-time time-dependent density functional theory

Elaheh Shomali, Markus E. Gruner ⬤, and Rossitza Pentcheva ⬤
*Department of Physics and Center for Nanointegration Duisburg-Essen (CENIDE), University of Duisburg-Essen,
Lotharstrasse 1, 47057 Duisburg, Germany*

The interaction of a femtosecond optical pulse with a Fe₁/(MgO)₃(001) metal/oxide heterostructure is investigated using time-dependent density functional theory calculations in the real-time domain. We systematically study electronic excitations as a function of laser frequency, peak power density, and polarization direction. While spin-orbit coupling is found to result in only a small time-dependent reduction of magnetization (less than 10%), we find a marked anisotropy in the response to in-plane and out-of-plane polarized light, which changes its character qualitatively depending on the excitation energy: the Fe layer is efficiently addressed at low frequencies by in-plane polarized light, whereas for frequencies higher than the MgO band gap, we find a particularly strong response of the central MgO layer for cross-plane polarized light. For laser excitations between the charge transfer gap and the MgO band gap, the interface plays the most important role, as it mediates concerted transitions from the valence band of MgO into the $3d$ states of Fe closely above the Fermi level and from the Fe states below the Fermi level into the conduction band of MgO. As these transitions can occur simultaneously without altering the charge balance of the layers, they could potentially lead to an efficient transfer of excited carriers into the MgO bulk, where the corresponding electron and hole states can be separated by an energy which is significantly larger than the photon energy.

I. INTRODUCTION

The recent development in brilliant ultrafast optical and x-ray sources with femtosecond resolution has fostered investigations that aim at a fundamental understanding of light-matter interaction and the resulting nonequilibrium properties of matter [1–7]. This paves the way for applications such as light-induced control of magnetization reversal for data storage [8,9] or light-induced hot carriers for photocatalytic processes, detection devices, and energy harvesting [10,11].

Time-dependent density functional theory (TDDFT) [12–14] in the real-time domain has evolved as an important tool to unravel the dynamics of excitation processes in organic and inorganic materials [7]. Recent efforts cover various aspects of light-matter interaction in metals [15,16] and semiconductors [17–19], the simulation of pump-probe experiments in Si [20] or nonlinear absorption in complex molecules [21], as well as charge and energy transfer after the impact of fast ions in aluminum sheets and nanoclusters [22–24].

Many potential applications of nonequilibrium states induced by laser pulses involve a combination of different materials, for instance in the field of photocatalysis [25,26] or optically induced (de)magnetization processes and spin transport in multilayer materials for magnetic storage [27,28]. In this spirit, not only experiment but also first-principles studies on optically excited systems in the real-time domain are shifting from single material and bulk systems towards

heterogeneous systems with increasing complexity. While a significant fraction of this research is concerned with the fundamental understanding of demagnetization processes in metallic multilayer systems [29,30], the photo-induced catalytic processes and energy conversion usually involve the transfer of energy and charge across interfaces [26,31]. In this context, real-time TDDFT (RT-TDDFT) approaches contribute towards a fundamental understanding of the carrier dynamics related to the plasmon-mediated injection of hot electrons from metallic nanostructures into semiconductors or insulators [32–35]. The efficient transfer of excitations or dissipation of energy across interfaces has also evolved as an important topic of ultrafast pump-probe experiments [3,36–38].

Understanding the interaction of laser pulses with a heterostructure offers the possibility to selectively induce excitations in a particular layer which may propagate into the entire system. At the interface between metallic and insulating layers, the electronic structure is characterized by the hybridization between orbitals of the metallic and insulating part, which usually leads to localized states within the gap in the adjacent layer of the insulator [36,39–41]. As we will show, these interface states might be employed by a proper choice of the photon energy to foster a simultaneous, concerted excitation of electrons and holes. This allows for a charge-neutral, but asymmetric, propagation of the excited carriers into the metallic and insulating subsystems. The symmetry breaking at the interface leads to splitting of states with in-plane and out-of-plane orbital character. As pointed out

earlier, changing the polarization of the incident light wave may result in a substantially different response [42], which could be used to select particular excitations at the interface and differentiate between the pathways of energy propagation into the bulk materials.

Fe/MgO(001) represents the ideal model system to explore such effects. The Fe/MgO system was extensively investigated in the context of tunnel magnetoresistance (TMR) and benefits from the fact that electronic, magnetic, and transport properties are well established [40,41,43–50]. Recently, optical and lattice excitations have also been subject to theoretical and experimental studies [36,42,51,52]. Bulk Fe is a ferromagnetic metal with bcc structure and a magnetic moment of $2.22 \mu_B$/atom [53], showing a substantial density of occupied and unoccupied d states in the vicinity of the Fermi level. MgO in turn is a wide-band-gap insulator, with an experimental band gap of about ~ 7.7 eV [54,55]). DFT calculations with local or semilocal exchange-correlation functionals yield 4.5–4.9 eV [56–59], but the band gap can be improved by using hybrid exchange-correlation functionals. For a correct description considering quasiparticle and excitonic effects is essential [60–62]. On the other hand, since quasiparticle corrections essentially lead to a rigid shift of the electronic states of the insulator [62] in MgO, semilocal functionals still allow for a qualitative analysis of the optical excitation processes.

Here, we investigate a minimum four-layer system $Fe_1/(MgO)_3(001)$ (see Fig. 1), which enables us to obtain a qualitative picture of the various types of excitations and the dynamics of excited carriers at the metal-insulator interface in the real-time domain. Despite its simplicity, our minimum model system already offers the necessary ingredients, such as a metallic and a nearly insulating layer separated by an interface layer characterized by a considerable hybridization between the $3d$ states of Fe and the $2p$ states of the apical oxygen, as illustrated in the layer- and orbital-projected density of states (DOS) in Fig. 1. We use a RT-TDDFT approach employing the adiabatic local density approximation (ALDA) for exchange and correlation for an adequate compromise regarding computational efficiency and numerical demand. Since our investigation is limited to the first 50 fs and photon energies far above the highest phonon modes, we neglect, at the current stage, ionic motion and electronic dissipation channels not covered by the ALDA.

In our previous investigation [42], we concentrated on optical excitations with laser frequencies up to 3.27 eV. These are still below the calculated bulk band gap of MgO obtained from (semi)local DFT calculations. These photon energies thus allow for excitations in the Fe layer that reach beyond the charge transfer gap, but not for direct excitation in MgO; see Fig. 1. In the present work, we now focus on laser frequencies in the vicinity and above the LDA band gap of MgO. We demonstrate that the excitation of the system (Fe vs MgO vs interface) depends strongly on the excitation energy and the polarization direction of the electric field. While the propagation of excited carriers across the interface could lead to the accumulation or depletion of charge in particular zones, we observe that interface-mediated simultaneous (but independent) excitation processes, involving electrons and holes, can effectively compensate the net charge transfer between the layers. In addition, we study the effect of field strength on the
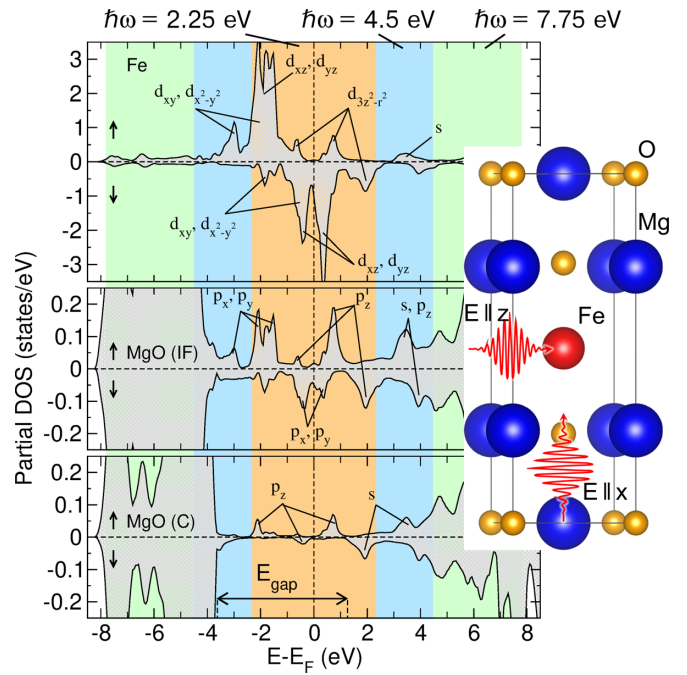

FIG. 1. Layer-resolved electronic density of states indicating the main orbital character of the states in the vicinity of the gap. The colored areas (orange for $\hbar\omega = 2.25$ eV, blue for $\hbar\omega = 4.5$ eV, green for $\hbar\omega = 7.75$ eV) mark the maximum energy range in which direct resonant excitations can be expected (i.e., from the occupied states at $-\hbar\omega$ to the Fermi level and from the Fermi level up to the unoccupied states at $\hbar\omega$). The horizontal arrow in the lowest panel denotes the position of the MgO band gap, obtained from the comparison of the bulk LDA band structure with the bands originating from the center layer of MgO [42]. Inset: Side view of the minimal heterostructure $Fe_1/(MgO)_3(001)$. The oscillating arrows illustrate the two orientations of the propagation direction of the applied laser pulses and the corresponding polarization of the electric field with respect to the layer stacking.

transfer of excitations and the impact of spin-orbit interaction (SOI), which results in transient changes in magnetization, arising from the optical excitation.

The paper is structured as follows: In Sec. II, we present the computational methodology and details. Section III A is devoted to magnetization dynamics, while in Sec. III B we compare the excitation patterns for three frequencies and in-plane polarization of the light field. Section III C addresses the dependence on the polarization direction of the electric field. Finally, Sec. IV provides a discussion and summary of the results.

II. COMPUTATIONAL DETAILS

The electronic structure and time-dependent properties were obtained from density functional theory (DFT) calculations using the ELK code [63], which is an all-electron full-potential linearized augmented plane-wave (LAPW) code that implements time-dependent DFT in the real-time (RT) domain. To model $Fe_1/(MgO)_3(001)$, we used muffin-tin radii of 1.139 Å, 1.164 Å, and 0.855 Å for Fe, Mg, and O, respectively. The plane-wave cutoff parameter, RK_{max}, was

set to 7. A $8 \times 8 \times 3$ k-mesh was used for the reciprocal space sampling. In the ground-state calculations, the convergence criterion for the electronic self-consistency cycle was a root-mean-square change of 10^{-7} a.u. in the Kohn-Sham potential. For the exchange-correlation functional, we have chosen the local (spin) density approximation (LDA) in the parametrization of Perdew and Wang (PW92) [64]. The optimized geometry [42] was previously obtained with the VASP code [65,66] using the generalized gradient approximation (GGA) of Perdew, Burke, and Ernzerhof (PBE) [67]. VASP (PBE) and ELK (LDA) lead to similar spin- and layer-resolved ground-state electronic partial DOS (PDOS) of the $Fe_1/(MgO)_3(001)$ heterostructure, which is shown in Fig. 1 (for more details, see [42]).

In our investigation, we simulate laser pulses with different laser frequencies and peak power densities but constant duration. The monochromatic electromagnetic wave is folded with a Gaussian envelope with a constant full width at half maximum (FWHM) of 5.81 fs. The peak of the pulse is reached at $t = 11.6$ fs after the start of the simulation.

The real-time TDDFT method propagates the electron density in time by integrating the time-dependent Kohn-Sham equation (TDKS) [29,68–71]. The electric field of the laser pulse, expressed by the vector potential, $\mathbf{A}_{ext}(t)$, enters the KS equation as a velocity gauge. By solving the TDKS equations, we can obtain the time-dependent electronic properties of a system such as time-dependent DOS (TDDOS), using the following equation (see Ref. [29]):

$$D_\sigma(E, t) = \sum_{i=1}^{\infty} \int_{BZ} d^3k \, \delta(E - \varepsilon_{i\mathbf{k}\sigma}) \, g_{i\mathbf{k}\sigma}(t), \qquad (1)$$

where $g_{i\mathbf{k}\sigma}(t)$ are the time-dependent and spin-resolved occupation numbers, defined as

$$g_{i\mathbf{k}\sigma}(t) = \sum_j n_{j\mathbf{k}\sigma} \left| \int d^3r \, \Phi_{j\mathbf{k}\sigma}(\mathbf{r}, t) \, \Phi_{i\mathbf{k}\sigma}^*(\mathbf{r}, 0) \right|^2. \qquad (2)$$

Here, $n_{j\mathbf{k}\sigma}$ is the occupation number of the jth orbital and Φ_i are the ground-state Kohn-Sham orbitals [69].

III. RESULTS

We carried out a systematic investigation of the impact of optical pulses with varying frequency, intensity, and polarization on a $Fe_1/(MgO)_3(001)$ heterostructure which consists of one layer of Fe and three layers of MgO: two interface (IF) and one central (C) in the latter, as illustrated in Fig. 1. Consistent with our previous study [42], the laser pulses were designed to achieve a fluency typically found in experiments [72,73] with a constant peak power density $S_{peak} \approx 5 \times 10^{12}$ W/cm^2 for most of our calculations. Additionally, we also applied pulses with $S_{peak} \approx 5 \times 10^{11}$ W/cm^2 and $S_{peak} \approx 5 \times 10^{10}$ W/cm^2, to assess nonlinear contributions (a detailed discussion is given in the Supplemental Material [74]). The shape of the laser pulses, as well as the Fourier transform of the time-dependent electric field, are shown in Fig. 2. Due to their finite duration, the pulses are not monochromatic and the Fourier transform of the time-dependent electric field $\mathbf{E}(t) = -\partial \mathbf{A}_{ext}(t)/\partial t$ is characterized by a Gaussian energy distribu-
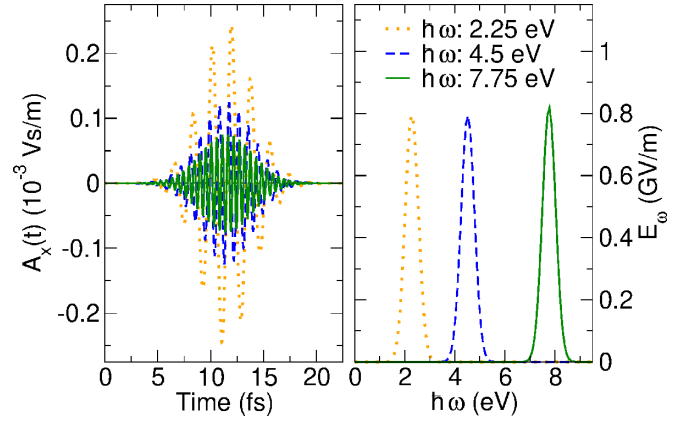

FIG. 2. Time-dependent vector potentials of laser pulses with different frequencies of $\hbar\omega = 2.25$ eV, $\hbar\omega = 4.5$ eV, and $\hbar\omega = 7.75$ eV (left) and Fourier transform of the time-dependent electric field for these laser pulses (right).

tion with a constant FWHM of 0.63 eV centered around the energy of the monochromatic light wave.

Our present investigation covers photon energies below ($\hbar\omega = 2.25$ eV), in the order of ($\hbar\omega = 4.5$ eV), and above ($\hbar\omega = 7.75$ eV) the LDA band gap of MgO (4.64 eV, consistent with previous results [56–59]), with particular emphasis on the impact of the polarization direction of the light wave relative to the orientation of the surface, as indicated by the oscillating red arrows in Fig. 1.

A. Magnetization dynamics

Beyond our previous work [42], here we include the spin-orbit interaction (SOI). With SOI, the z component of the electronic spin is no longer a conserved quantity, and thus the laser excitation may impact the magnetization of the system. We expect the largest effect for Fe, which in the ground state carries a moment of 2.25 μ_B (close to the experimental value for bulk bcc iron, 2.22 μ_B [53]) and provides nearly the complete magnetization of the system, whereas on the neighboring O and Mg IF sites, there is only a small induced spin polarization of 6.4×10^{-4} μ_B and 1.3×10^{-2} μ_B, respectively. The time-dependent change of the total magnetization (cf. Fig. 3) shows dependence on the laser frequency as well as polarization, but remains with, at most, $\Delta m = -0.15$ μ_B, which is small compared to the total moment in the cell. For an in-plane orientation of the electric field vector, the largest decrease is observed for a photon energy of 2.25 eV, with its maximum change around 40 fs after the start of the pulse and a steady recovery afterwards. With increasing photon energies, the effect is even smaller and the maximum change is reached earlier in time. This is attributed to the fact that the d electrons, responsible for the large spin polarization, are more efficiently addressed by the lower energy pulses. For a polarization of the electric field along the stacking direction of the layers, the response of the magnetic subsystems is weaker with minute changes in magnetization for the photon energy of 4.5 eV and somewhat larger for 7.75 eV ($\Delta m = -0.05$ μ_B). Thus, we conclude that SOI has only a minor impact on the dynamics of charge transfer and excitations across the
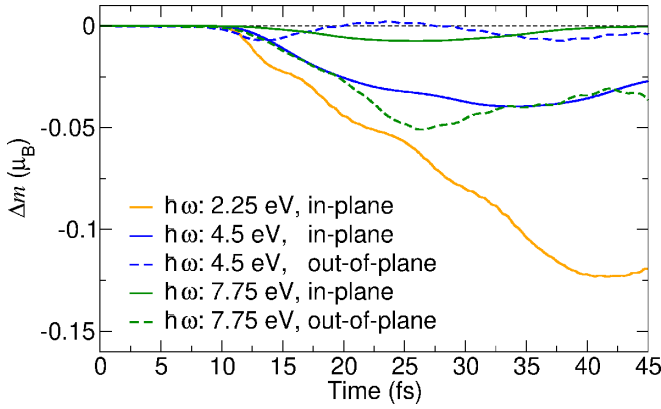
FIG. 3. Change of the total magnetic moment in the simulation cell as a function of time for in-plane and out-of-plane laser pulses with different laser frequencies.

FIG. 4. Changes in the charge distribution $\Delta\rho(\mathbf{r}, t) = \rho(\mathbf{r}, t) - \rho(\mathbf{r}, 0)$ at $t = 20.2$ fs after illumination with an in-plane polarized laser pulse with $S_{\text{peak}} \approx 5 \times 10^{12}$ W/cm^2 for (a) $\hbar\omega = 2.25$ eV, (b) $\hbar\omega = 4.5$ eV, and (c) $\hbar\omega = 7.75$ eV. Red/blue isosurfaces indicate regions with a depletion/accumulation of charge with an isosurface level of $\pm 2 \times 10^{-3} e_0/a_B^3$.

interface in Fe$_1$/(MgO)$_3$(001). This is further supported by a detailed comparison of the time- and layer-resolved DOS for two relevant cases in the Supplemental Material [74], which does not exhibit a notable difference between the excitation patterns obtained with SOI and within the scalar-relativistic approach. The limited impact of the laser pulse on the magnetization dynamics indicates that the mixing between the spin channels is small and thus the z component of the spin is rather conserved. This allows us to use the differences between the spin-up and -down projected time-resolved DOS to identify the propagation of excitations from the strongly spin-polarized Fe layer to the non-spin-polarized MgO part. However, further studies involving thicker heterostructures may be necessary to address other relevant mechanisms that can lead to laser-induced magnetization reversal such as the optically induced spin transfer (OISTR) mechanism [29], observed in combined ferro-/antiferromagnetic heterostructures.

B. Laser excitations below and above the MgO gap

In the following, we will address how the response of a metal/insulator heterostructure depends on the frequency of the electromagnetic wave. We elucidate different scenarios in our RT-TDDFT simulation by applying three different laser pulses with the same shape and peak power density, $S_{\text{peak}} \approx 5 \times 10^{12}$ W/cm^2, as in the previous section, but with different excitation energies $\hbar\omega = 2.25$, 4.5, and 7.75 eV, covering the relevant range of photon energies. We start with the electric field of the pulse oriented along the x axis, i. e., parallel to the stacking plane. The first energy, $\hbar\omega = 2.25$ eV, is clearly below the band gap and can only address interface states in the MgO part or the conduction band across the charge transfer gap.

The second energy of 4.5 eV falls slightly short of the LDA band gap of 4.64 eV. Although the finite pulse width leads to a Gaussian distribution of energies with a tail above this value (cf. Fig. 2), direct excitations across the gap are negligible. The largest energy, $\hbar\omega = 7.75$ eV, is, on the other hand, sufficient for optical excitations in bulk MgO (see Fig. S3 in the Supplemental Material [74] for a comparison of the response of bulk MgO to pulses with $\hbar\omega = 4.5$ and 7.75 eV).
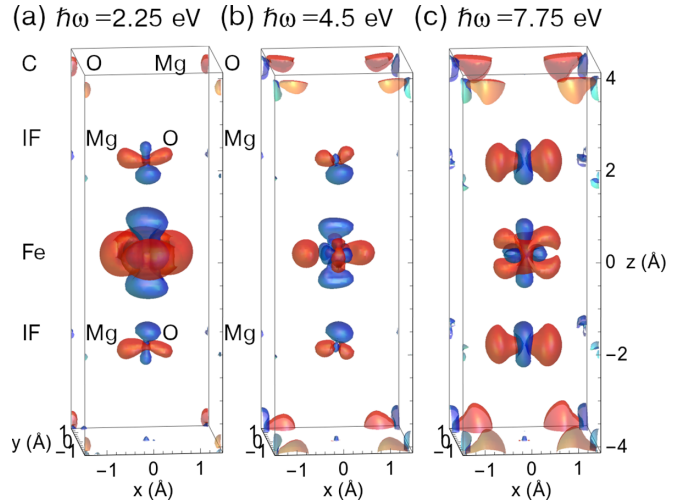
The transient charge redistribution in the Fe/MgO heterostructure, $\Delta\rho(\mathbf{r}, t) = \rho(\mathbf{r}, t) - \rho(\mathbf{r}, 0)$, shown in Fig. 4 for the three excitation energies at $t = 20.2$ fs, right after the decay of the laser pulse, provides a spatially resolved illustration of the characteristic features and differences. For all three frequencies, only small features show up at the Mg sites, indicating the primary importance of Fe and O orbitals. The changes in the charge cloud around the central Fe atom are largest for $\hbar\omega = 2.25$ eV, while for $\hbar\omega = 7.75$ eV, we see enhanced excitations in the MgO layers, in accordance with our considerations from the last paragraph. The isosurfaces for $\hbar\omega = 2.25$ and 4.5 eV indicate a transfer of charge mainly from in-plane ($d_{x^2-y^2}$ and/or d_{xy}) to $d_{3z^2-r^2}$ orbitals of Fe. Likewise, at the apical O(IF), a transfer from in-plane oriented p_x to out-of-plane p_z orbitals takes place. For $\hbar\omega = 7.75$ eV the pattern in $\Delta\rho(\mathbf{r}, t)$ rather suggests a transfer from d_{xz} and d_{yz} to $d_{3z^2-r^2}$ and in-plane d orbitals at the Fe site, whereas at O(IF) and O(C), a rather symmetric and much larger pattern emerges, indicating again a significant transfer from in-plane to out-of-plane oriented p orbitals. To address the question of whether the excitations are coupled or occur independently in each layer, we compare in Fig. 5 the change in the spin- and layer-resolved projected time-dependent DOS, $\Delta D_\sigma(E, t) = D_\sigma(E, t) - D_\sigma(E, 0)$, for the three cases. For the lowest frequency $\hbar\omega = 2.25$ eV, we consistently observe the largest changes in the minority spin channel of the Fe layer, as it offers in comparison to the majority channel a larger number of potential initial and final states. Most of the features can be traced back to direct resonant transitions from occupied to unoccupied states in the static DOS, but several features also appear at energies significantly above and below the Fermi level. Such excitations are in particular present in both MgO layers, for instance close to the valence band edge of MgO, which lies around 4 eV below the Fermi level in the present heterostructure, suggesting a multiphoton excitation process.
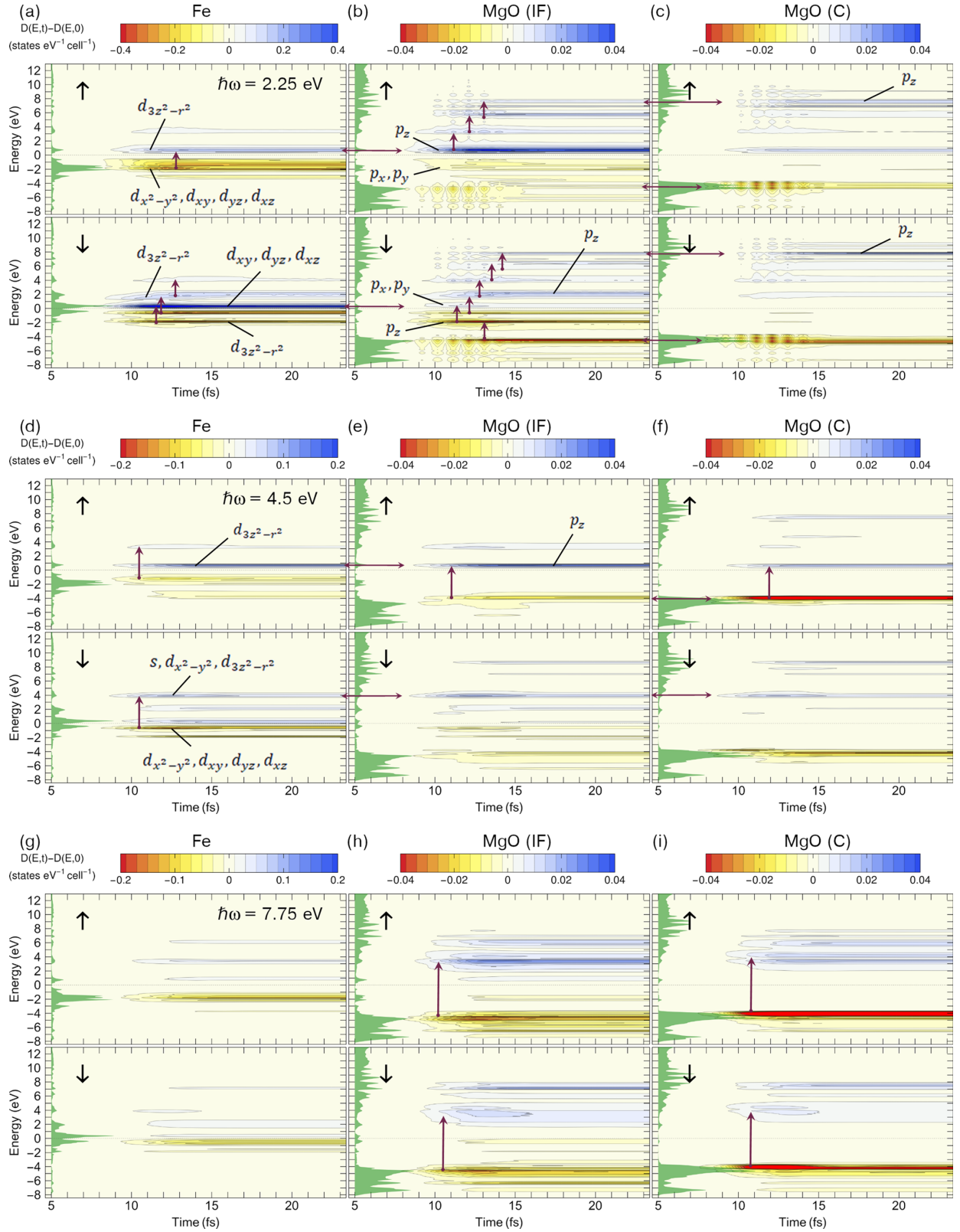
FIG. 5. Time-dependent changes in the layer-resolved ΔTDDOS for three in-plane laser pulses with frequencies (a)–(c) $\hbar\omega = 2.25$ eV, (d)–(f) $\hbar\omega = 4.5$ eV, (g)–(i) $\hbar\omega = 7.75$ eV, and a peak power density of $S_{\text{peak}} \approx 5 \times 10^{12}$ W/cm^2. The three columns show the partial $\Delta D_\sigma(E, t)$ of the Fe, the IF-MgO, and the center-MgO layers, respectively. The energy E is given relative to the Fermi level. Note that the color scale differs between the columns. Purple arrows mark particular transitions and hybridizations, which are discussed in the text. The green area at the left edge of each panel shows the static ground-state partial density of states for the respective layer. For better visibility, the static DOS of the MgO layers in the center and right column is scaled by a factor 4 compared to Fe in the left column.

These excitation patterns disappear when the intensity of the pulse—specified here in terms of its peak power density—is reduced by one or two orders of magnitude, while the features within $\pm\hbar\omega$ from E_F are still present (see Figs. S6 and S7 in the Supplemental Material [74] for a detailed discussion). This proves that the features far away from E_F arise from nonlinear processes, while resonant excitations in the vicinity of E_F remain the main channel for carrier excitation. This indicates in turn that nonlinear excitation effects in sufficiently strong pulses may be employed to effectively (de)populate spatially extended states in the valence or conduction band of MgO(IF) and MgO(C) at energies beyond the range of a direct excitation. Thus, for MgO(C), a significant depletion of valence band states takes place between -4 and -5 eV, almost as large as in MgO(IF). Likewise, we observe connected features at $+8$ eV, both indicated by the horizontal arrows in Figs. 5(b) and 5(c). In MgO(C), intermediate levels, from which carriers might be excited beyond the gap, are essentially absent owing to the exponential decay of interface states in the band gap with increasing distance from the interface. Nevertheless, the changes in occupation numbers in the valence and conduction bands are even larger in the central layer compared to the interface.

The resonant excitations in the vicinity of the Fermi level confirm our previous conjecture that hybridization between out-of-plane oriented orbitals in adjacent layers is particularly relevant for the transfer of excitations into and through the interface [42]; see Figs. 5(a)–5(c). Because of the large exchange splitting, unoccupied $d_{3z^2-r^2}$ states of Fe in the majority spin channel are located $+0.8$ eV above E_F, that can be reached by electrons transferred from in-plane d orbitals around -1.5 eV below E_F [vertical arrows in Fig. 5(a)]. The Fe $d_{3z^2-r^2}$ states hybridize with the p_z orbitals of MgO(IF), which show a significant occupation as well in this energy range. In contrast, the decrease in occupation of the p_x and p_y states in MgO(IF) around -1.5 eV appears much weaker, in particular compared to the rather strong effect in the $d_{x^2-y^2}$ and d_{xy} orbitals of the Fe layer found at the same energy. In the minority channel, the out-of-plane oriented bonding $d_{3z^2-r^2}$ states at -2 eV mediate the excitation of carriers from the O p_z states in the interface to the Fe d_{xz} and d_{yz} states around $+0.5$ eV, which hybridize with the in-plane oriented p_x and p_y interface states in MgO(IF); see the horizontal arrows in Figs. 5(a) and 5(b). Their occupation is much lower compared to the out-of-plane p_z states in the majority channel in the same energy range.

The excitation pattern becomes more defined when we increase the energy towards the band gap of MgO. Due to the confined width of the d band in the Fe monolayer, the number of matching initial and final states for excitations within the d band of Fe is diminished. For $\hbar\omega = 4.5$ eV, our simulations do not yield significant direct excitations between the valence and conduction band states in bulk MgO. Thus, at this energy, we can pinpoint the interface layer as pivotal for the excitations. We still observe in all layers a different excitation pattern in the minority and majority channel arising from the proximity to the spin-polarized Fe layer. In the majority channel, carriers from the delocalized valence band edge of MgO(IF) and MgO(C) are excited into unoccupied interface states at $+0.5$ eV, which hybridize with the $d_{3z^2-r^2}$

states in the Fe layer. In the minority channel, we observe a similar mechanism as described above, which effectively relocates the charge density in the reverse direction, towards MgO. It involves the $d_{3z^2-r^2}$ states of Fe which hybridize with the conduction band states of MgO(IF) and MgO(C); see Figs. 5(d) and 5(e).

If we take a separate look at the central layer in Fig. 5(f), we observe depletion of states at the valence band edge of MgO(C) and a concomitant occupation in the conduction band separated by almost twice the laser energy. The comparison with our calculations for MgO bulk (cf. Fig. S3(b) in the Supplemental Material [74]) prove that the intensity of the excitation cannot be explained by a direct transition in bulk MgO. Instead, the IF layer plays a decisive role, as it mediates concerted excitations from the valence band states extending between MgO(IF) and MgO(C) to the hybridized states of MgO(IF) and Fe just above the Fermi level and, simultaneously, hybridized states of MgO(IF) and Fe just below the Fermi level to the extended conduction band states in MgO(IF) and MgO(C). These processes work in opposite directions and can be invoked independently by the same laser pulse. Their combination prevents an effective charge transfer between the metallic and the insulating subsystem.

For $\hbar\omega = 7.75$ eV, a substantial laser excitation can occur directly in the MgO subsystem without the support of interface states. As a consequence, the excitation patterns of both spin channels assimilate in both layers of MgO, as compared to the lower photon energies. The largest fraction of the excitations removes states from the first peak below the valence band edge at -4 eV (corresponding to -1.2 eV in bulk MgO) and populates states around 3.5–4.0 eV (corresponding states in bulk MgO are located around 6.5 eV; see Fig. S3(a) in the Supplemental Material [74]), which are marked by the vertical arrows in Figs. 5(g)–5(i). Direct excitations in the Fe layer, as observed for the smaller frequencies, are largely absent. The substantial changes in the occupation numbers in Fe close to the Fermi level are again best explained through the interface-mediated mechanisms discussed above, which originate from the hybridization between the spin-polarized states in Fe with MgO(IF). Despite the largest amount of excitation taking place directly in MgO(IF) and MgO(C), there is still some remaining asymmetry between the spin channels visible in Fig. 5(i). This asymmetry is a consequence of the participation of the spin-polarized metal layer since the corresponding static DOS of both spin channels is rather similar (cf. the green areas in Fig. 5).

C. Polarization dependence of the excitation pattern

The diagonal components of the imaginary part of the dielectric tensor Im[$\epsilon(\omega)$], reported previously [42], indicate a predominance of in-plane components for low excitation energies and a substantial increase of absorption in the z direction for frequencies above the band gap of MgO. In particular, we found that for our system, the in-plane component Im[$\epsilon_{xx}(\omega)$] resembles bulk Fe, while the out-of-plane component Im[$\epsilon_{zz}(\omega)$] rather bears similarity to bulk MgO, in particular regarding the low absorption at energies below the gap. This implies a strong dependence of the excitation pattern
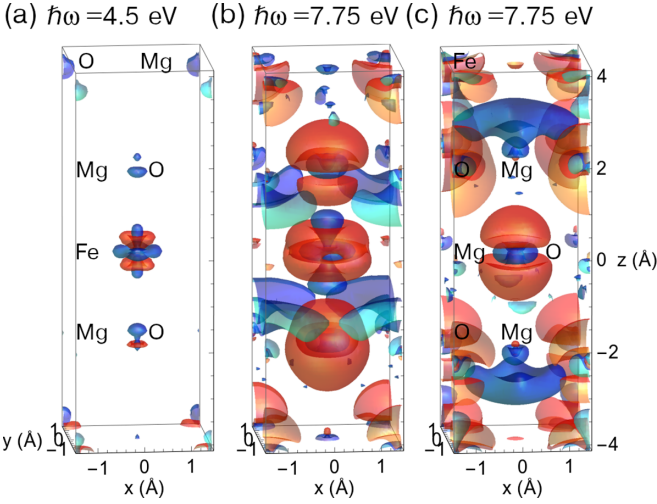
FIG. 6. Snapshot of the evolution of the charge distribution $\Delta\rho(\mathbf{r}, t)$ for out-of-plane polarized pulses at $t = 20.2$ fs for (a) $\hbar\omega = 4.5$ eV and (b) $\hbar\omega = 7.75$ eV. Same colors and isolevels as in Fig. 4. The positions of the atoms in the cell in (a) and (b) are the same as in Fig. 1 with Fe in the center. In (c), we shift the differential charge distribution shown in (b) by one half lattice vector in each direction, in order to better visualize the features at the edges of the original unit cell. As a result, O(C) is now located in the center, while Fe is placed at the edges of the cell.

on the polarization of the electric field component of the light pulse.

To assess this, we carried out additional RT-TDDFT simulations for $\hbar\omega = 4.5$ eV and 7.75 eV with the vector potential (and thus the electric field) pointing along the z axis, i.e., along the stacking sequence of the heterostructure. The peak power density $S_{\text{peak}} \approx 5 \times 10^{12}$ W/cm^2 and pulse shape were kept the same as in the last section. The corresponding electron density differences taken at 20.2 fs are shown in Fig. 6. They exhibit, indeed, substantial differences to the in-plane polarized field, but also between the two laser frequencies. At 4.5 eV, we observe a much weaker response compared to

the in-plane case, which mainly involves a redistribution of charge from d_{xz} and d_{yz} to $d_{3z^2-r^2}$ and $d_{x^2-y^2}$ orbitals at Fe [cf. Fig. 6(a)], similar to what was found for $\hbar\omega = 1.67$ eV in Ref. [42]. In contrast, Figs. 6(b) and 6(c) show a substantially increased charge redistribution at all sites in the unit cell for the out-of-plane polarized 7.75 eV pulse as compared to its in-plane counterpart [cf. Fig. 4(c)]. At the Fe site, we monitor once again an occupation of $d_{3z^2-r^2}$ states and a depletion of orbitals with in-plane character, whereas the pattern at the apical and central O sites suggests a redistribution between the s and p_z orbitals. In contrast to frequencies below the bulk band gap of MgO, we encounter rather significant changes in the charge distribution around Mg(IF) sites as well. These effects are rather asymmetric and extend towards the Fe site into the interstitial.

The characteristic features of the differential charge density $\Delta\rho$ are also reflected in the integrated charge density ΔQ in the muffin-tin spheres around each site, shown in Fig. 7(a). We encounter, for all frequencies and both directions of polarization, a steep change in ΔQ at the onset of the pulse, reaching a steady value after the pulse. At the O sites, we see a corresponding decrease in ΔQ, accompanied by an increase of similar magnitude at the Mg sites, which we previously interpreted as an effective charge transfer from O to Mg [42]. Consistently, this charge transfer increases significantly for $\hbar\omega = 7.75$ eV, where direct excitations within bulk MgO occur. For the out-of-plane polarized pulse, the increase of charge around Mg(IF) is significantly larger than the decrease around O(IF). Simultaneously, the amount of charge leaving the muffin-tin sphere of Fe has substantially increased. This suggests that the large blue features close to Mg(IF) in Fig. 6(c) arise from a relocation of charge from the d orbitals of Fe.

The ΔQ are modulated by an oscillation with twice the frequency of the laser excitation, alluding to a coherent ringing of the charge clouds which extends until the end of our simulations at 45 fs. This is combined with characteristic beats, indicating the superposition of oscillations with slightly varying frequencies. The frequency doubling is a consequence
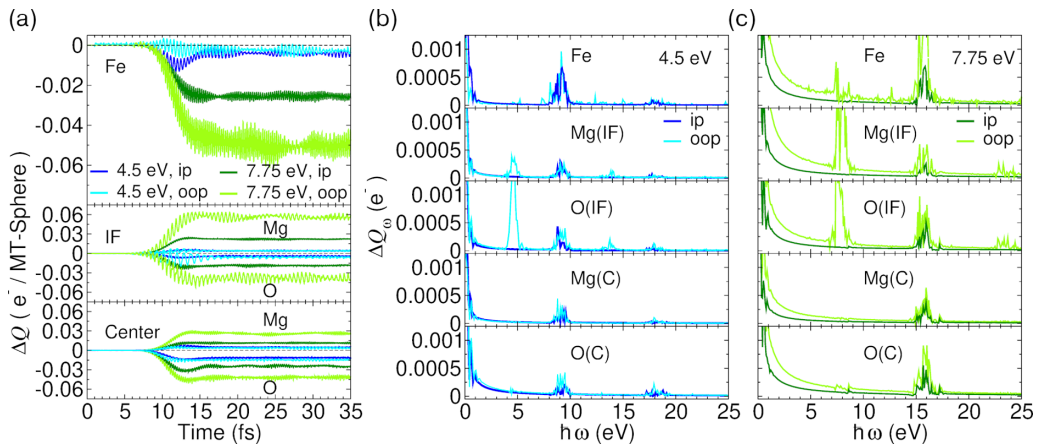

FIG. 7. (a) Change of the electronic charge inside the muffin-tin spheres around the ions relative to the initial state, $\Delta Q(t) = Q(t) - Q(0)$, during and after the application of in-plane (ip) and out-of-plane (oop) polarized laser pulses with $\hbar\omega = 4.5$ eV and $\hbar\omega = 7.75$ eV. The initial charges $Q(0)$ within the muffin-tin spheres for Fe, Mg(IF), O(IF), Mg(C), and O(C) are 24.42 e_0, 10.67 e_0, 7.24 e_0, 10.72 e_0, and 7.24 e_0, respectively. (b),(c) Fourier transform of $\Delta Q(t)$ shown in (a) for $\hbar\omega = 4.5$ eV and $\hbar\omega = 7.75$ eV, respectively.
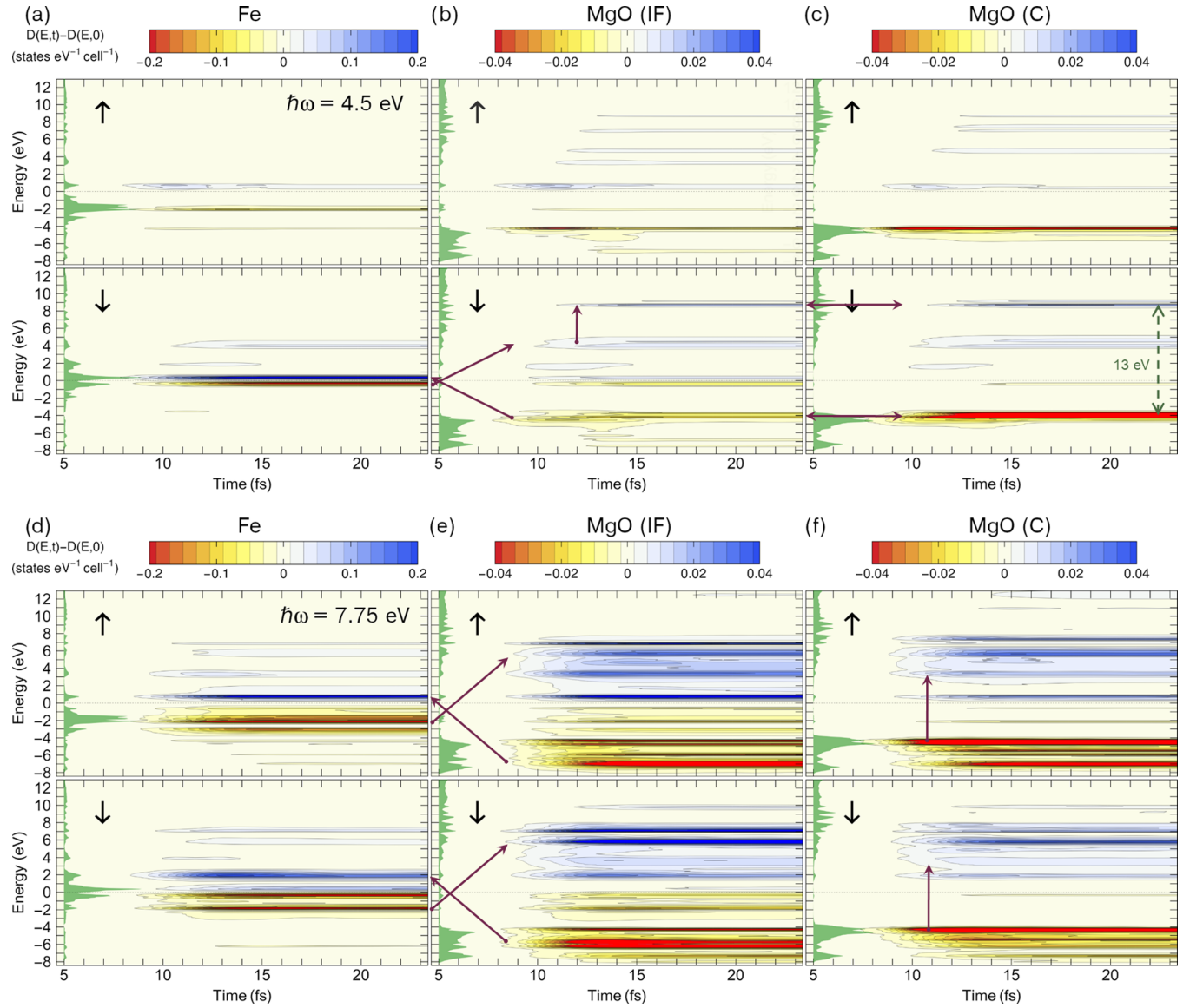
FIG. 8. Time-dependent changes in the layer-resolved ΔTDDOS for out-of-plane laser pulses with frequencies (a)–(c) $\hbar\omega = 4.5$ eV and (d)–(f) $\hbar\omega = 7.75$ eV and a peak power density of $S_{\text{peak}} \approx 5 \times 10^{12}$ W/cm^2. The three columns show the partial $\Delta D_\sigma(E, t)$ for the Fe, MgO(IF), and MgO (C) layers, respectively. The energy E is given relative to the Fermi level. Note that the color scale differs between the columns. Purple arrows mark particular transitions and hybridizations, which are discussed in the text. The green areas again refer to the static partial DOS, scaled as in Fig. 5.

of the electric field driving the charge out and back into the muffin-tin sphere at both sides in a similar way at positive and negative amplitudes. This symmetry is, however, broken at the interface for out-of-plane oriented pulses and the oscillations for Mg(IF) and O(IF) exhibit only half the frequency of the Fe and the central layers of MgO, accordingly. This is substantiated by the Fourier transform $\Delta Q(\omega)$ shown in Figs. 7(b) and 7(c) for $\hbar\omega = 4.5$ eV and $\hbar\omega = 7.75$ eV, respectively. All curves show a large contribution at $\omega = 0$ and features at $2\hbar\omega$ with a finite extension, similar to the width of the laser pulse. The latter can explain the beating in the oscillations in $\Delta Q(t)$. For $\hbar\omega = 4.5$ eV, we also observe higher harmonics at $4\hbar\omega$, which appear most pronounced for O(C). In addition, the out-of-plane polarized pulses shown in Figs. 7(b) and 7(c) exhibit large peaks at $\hbar\omega$ with a satellite at $3\hbar\omega$, in particular

in the interface MgO layer. These peaks are suppressed in Fe and the central layer of MgO, both of which have mirror symmetry.

The particular role of the interface for the excitation is even more pronounced for the out-of-plane polarization of the electric field, as shown in Fig. 8. Most conclusive, once again, is the minority channel, where occupied and unoccupied d states of Fe are nearly balanced. For $\hbar\omega = 4.5$ eV, we find two pronounced and rather sharp features above and below the Fermi level, which are too close together to be explained by resonant excitations within the Fe layers; see Fig. 8(a). However, taking into account that these features hybridize with interface states in MgO(IF), we can conjecture once again two transitions taking place cooperatively, which result in an effective transfer between the $3d$ orbitals of Fe: one from the valence band

of MgO into the interface states above E_F and another one from the interface states below E_F into the conduction band of MgO; see Figs. 8(a) and 8(b). The latter is involved in a subsequent nonlinear excitation process, populating the MgO levels at 8.5 eV. Furthermore, we observe similar features with larger changes in the occupation numbers above and below the Fermi level for the central layer of MgO [see Fig. 8(c)], keeping in mind that 4.5 eV is not yet sufficient for a substantial direct excitation across the band gap. Interestingly, in MgO(C), the population of the unoccupied states at 8.5 eV appears to be even more defined compared to the pattern at 4 eV, which we can link to a direct excitation in the IF layer. This indicates that excitations in the nonlinear regime may actively foster the transfer of excitations across the IF.

As expected from the differential charge density and the larger absorption coefficient for out-of-plane light, $\hbar\omega = 7.75$ eV leads in all three distinct layers to a much richer pattern in $\Delta D(E, t)$. In Fig. 8(f), which refers to MgO(C), the vertical arrows denote the corresponding transition from the valence to the conduction band in bulk MgO. Excitations above $+6$ eV and below -6 eV apparently involve transitions to and from the interface states of MgO(IF). Consequently, we see changes in the occupation numbers of MgO(IF) and Fe, which are consistent with the mechanism identified above: from approximately -6 eV to $+1\ldots2$ eV and from -2 eV and above to $+6\ldots7$ eV, as indicated by the diagonal arrows in Figs. 8(d) and 8(e). Excited carriers at the lowest and the highest energies accumulate exclusively in MgO(IF) and MgO(C), while the hybridizing d states of Fe, which provide a large density of states can serve as a buffer in the vicinity of the Fermi energy for the excitations from and into the MgO subsystem.

The combination of a d metal and a wide-band-gap insulator leads thus not only to a transfer of excited carriers into the subsystems, but also to an asymmetric transfer of energy. In the Fe layer, due to its metallic nature and the confinement, excited electron and hole states lie closer together than the photon energy. The distribution of excitations is thus closer to thermalization than one would obtain from an excitation of bulk Fe with the same light pulse. In contrast, excited positive and negative carriers are separated by up to 13 eV in MgO(C) for a strong 4.5 eV light pulse.

IV. DISCUSSION AND CONCLUSION

Our systematic RT-TDDFT investigation of a minimal model Fe/MgO heterostructure shows that the response of the system strongly depends on both the photon frequency and polarization of the light field. Moreover, we could unravel the origin of the excitation and the transfer of carriers in full detail. In contrast to our previous study on $Fe_1/(MgO)_3(001)$, we considered spin-orbit interactions and found that demagnetization effects do not exceed 10% of the ground-state magnetization of the Fe layer and can thus be regarded to be of minor relevance in this particular system.

We find in accordance with our previous study that for photon energies substantially below the LDA band gap of MgO, excitations take place predominantly in the Fe subsystem, which provides a rich variety of initial and final states within the width of the d band. This works most effectively
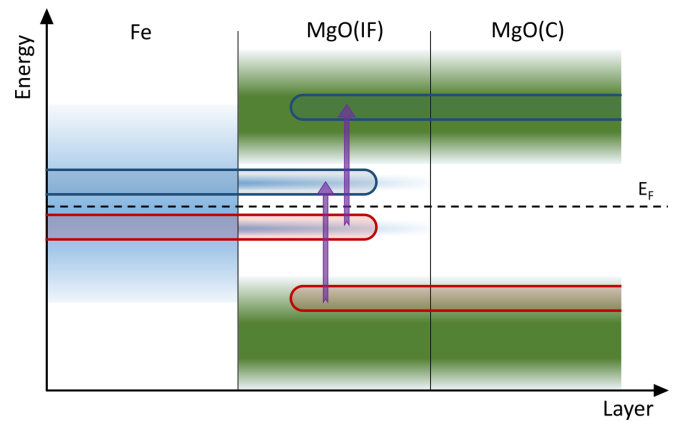

FIG. 9. Schematic illustration of the concerted excitation mechanism mediated by interface states involving two simultaneous, but independent excitations across the charge transfer gap. This leads to the accumulation of excited carriers with a small energy separation in the metallic layer and a significantly larger separation than $\hbar\omega$ in the MgO part. In this way, an efficient repopulation of carriers from valence band (red frame) to conduction band states (blue frame) is possible even for photon energies below the band gap of the insulator. The colored areas refer to the electronic bands. Green: valence and conduction bands of the (bulk) insulator; blue: d states of the (bulk) metal and interface states.

when the electric field component of the light lies within the plane of the Fe layer. The situation changes drastically when the photon energy approaches or even exceeds the LDA band gap of MgO. The reduced dimension of the Fe layer narrows the d-band width of the Fe monolayer compared to bulk, with the consequence that even photon energies around 4.5 eV (i.e., close to the LDA band gap of MgO) can hardly trigger substantial excitations within the Fe layer. Thus, for frequencies in the order of the d-band width and larger, the hybridization of Fe-d and O-p states at the interface plays a decisive role for the excitation.

Hence, we could identify a generic mechanism associated with these states, which allows one to pump excitations from deep within the valence band into the conduction band of the insulator even when the photon energy is not sufficient to reach the final states through direct excitation. This mechanism involves two simultaneous (but not necessarily coherent) excitations in the interface region; see Fig. 9. The first excites valence band electrons of the insulator into an interface state above the Fermi level, while the second promotes electrons from the interface states below the Fermi level into the conduction band of MgO. The interface states of oxygen usually exhibit a low DOS, but since they hybridize with the d states of the transition metal, the latter can act as a reservoir to accept and donate excited carriers to the apical oxygen. In turn, the relevant excitations in the valence and conduction bands can extend into the bulk layers of MgO, where direct transitions are inhibited by the band gap. Although this takes place independently, hot electrons and holes obtained from the two processes might thus be observed simultaneously in the bulk of the insulator, avoiding the penalty related to the Coulomb interaction between charged zones. Indeed, we found clear indications of

such a joint accumulation of excited holes and electrons in the central layer. Whether a likewise transfer of excitations can be observed from the interface layer of Fe into the bulk needs to be assessed in future studies for thicker Fe films. Here, again, a sufficient hybridization of the out-of-plane d orbitals between the inner Fe layers and the IF states might be a decisive factor. The above described mechanism leads to an asymmetric distribution of excitations, where—directly after the pulse—the excited electrons and holes in the metal are much closer to the Fermi level, as compared to the MgO subsystem. This might then lead to a substantially different dynamics of thermalization in both subsystems of the heterostructure as compared to the respective bulk systems, which might be detectable in time-resolved pump-probe experiments on the fs timescale. Sufficiently high laser intensities, as applied in our computational approach, can furthermore trigger a non-linear multiphoton excitation process that allows one to reach hybridized valence and conduction band states with a significantly larger distance to the Fermi level as compared to the photon energy. This implies that a similar effect might be achieved by the simultaneous application of two weaker laser pulses with different, appropriately chosen frequencies.

Our simulations indicate a strong dependence of the absorbed light on the polarization of the electrical field and the frequency. As a consequence, the polarization direction emerges as an efficient means to select transitions to specific interface states. For frequencies below the band gap, in-plane polarized light induces a much stronger absorption, as shown previously [42], whereas for photon energies above the band gap, the out-of-plane direction leads to a significantly larger response. While in the former case excitations are confined to the Fe layer, the direct excitations within the MgO play the most important role in the latter since the finite width of the Fe-d band limits the number of possible transitions in the ultrathin Fe layer. For photon energies in the order of the band gap, we found excitations of similar strength for both polarization directions. Still we can distinguish these cases by a different excitation pattern in Fe and the adjacent MgO layer. We link this to the local symmetry breaking at the interface, leading to an asymmetric deformation of the atomic charge cloud, which follows the oscillation of the vector potential.

Our calculations were carried out for a minimal model heterostructure, but we believe that the above sketched mechanisms can also be transferred to larger, more realistic systems with nanometer-sized layers, as used in previous experiments [36]. An important consequence of the confinement is the significantly reduced bandwidth of the 3d-metal monolayer. A wider d band would provide, according to Fermi's golden rule, additional possibilities for direct excitations within the Fe subsystem for a laser pulse in the range of the calculated band gap. On the other hand, the MgO band gap is underestimated due to the LDA exchange-correlation functional. Thus, for a direct comparison with experiment, a quantitative description of the band gap and the location of the interface states is desirable. This requires the appropriate treatment of exchange and correlation beyond the (adiabatic) local density approximation in a time-dependent approach for both the ferromagnetic metal and the insulator in a computationally efficient implementation and needs to be assessed in future work.

Despite the above-mentioned restrictions, the model used in this study captures the essential excitation processes that may also be relevant for thicker heterostructures, when a laser pulse is applied with photon energy, which is slightly lower than the band gap of the insulator, but in the vicinity of or even larger compared to the d-band width of the metal. We expect that the fundamental mechanisms of excitation dynamics demonstrated in our proof-of-principle calculations are applicable to a wider range of metal-insulator heterostructures, which are characterized by a large density of states around the Fermi level in the metallic subsystem, and thus provide important guidelines for future pump-probe experiments.

[1] A. Cavalleri, M. Rini, H. H. W. Chong, S. Fourmaux, T. E. Glover, P. A. Heimann, J. C. Kieffer, and R. W. Schoenlein, Phys. Rev. Lett. **95**, 067405 (2005).

[2] R. Ernstorfer, M. Harb, C. T. Hebeisen, G. Sciaini, T. Dartigalongue, and R. J. D. Miller, Science **323**, 1033 (2009).

[3] A. Melnikov, I. Razdolski, T. O. Wehling, E. T. Papaioannou, V. Roddatis, P. Fumagalli, O. Aktsipetrov, A. I. Lichtenstein, and U. Bovensiepen, Phys. Rev. Lett. **107**, 076601 (2011).

[4] S. Ichikawa, H.and Nozawa, T. Sato, A. Tomita, K. Ichiyanagi, M. Chollet, L. Guerin, N. Dean, A. Cavalleri, S. Adachi, T. Arima, H. Sawa, Y. Ogimoto, M. Nakamura, R. Tamaki, K. Miyano, and S. Koshihara, Nat. Mater. **10**, 101 (2011).

[5] L. Stojchevska, I. Vaskivskyi, T. Mertelj, P. Kusar, D. Svetin, S. Brazovskii, and D. Mihailovic, Science **344**, 177 (2014).

[6] H. Hübener, M. A. Sentef, U. De Giovannini, A. F. Kemper, and A. Rubio, Nat. Commun. **8**, 13940 (2017).

[7] J. Lloyd-Hughes, P. Oppeneer, T. P. dos Santos, A. Schleife, S. Meng, M. A. Sentef, M. Ruggenthaler, A. Rubio, I. Radu, M. Murnane, X. Shi, H. Kapteyn, B. Stadtmüller, K. M. Dani, F. da Jornada, E. Prinz, M. Aeschlimann, R. Milot, M. Burdanova, J. Boland *et al.*, J. Phys.: Condens. Matter **33**, 353001 (2021).

[8] C. Stamm, T. Kachel, N. Pontius, R. Mitzner, T. Quast, K. Holldack, S. Khan, C. Lupulescu, E. F. Aziz, M. Wietstruk, H. A. Dürr, and W. Eberhardt, Nat. Mater. **6**, 740 (2007).

[9] I. Radu, K. Vahaplar, C. Stamm, T. Kachel, N. Pontius, H. A. Duerr, T. A. Ostler, J. Barker, R. F. L. Evans, R. W. Chantrell, A. Tsukamoto, A. Itoh, A. Kirilyuk, T. Rasing, and A. V. Kimel, Nature (London) **472**, 205 (2011).

[10] M. L. Brongersma, N. J. Halas, and P. Nordlander, Nat. Nanotechnol. **10**, 25 (2015).

[11] P. Narang, R. Sundararaman, and H. A. Atwater, Nanophotonics **5**, 96 (2016).

[12] *Fundamentals of Time-dependent Density Functional Theory*, edited by M. Marques, N. Maitra, F. M. S. Nogueira, E. K. U. Gross, and A. Rubio (Springer, Berlin, 2012).

[13] S. Sharma, J. Dewhurst, and E. Gross, Top. Curr. Chem. **347**, 235 (2014).

[14] V. Olevano, *Structures on Different Time Scales* (De Gruyter, Berlin, 2018), pp. 101–142.

[15] M. Volkov, S. A. Sato, F. Schlaepfer, L. Kasmi, N. Hartmann, M. Lucchini, L. Gallmann, A. Rubio, and U. Keller, Nat. Phys. **15**, 1145 (2019).

[16] R. D. Senanayake, D. B. Lingerfelt, G. U. Kuda-Singappulige, X. Li, and C. M. Aikens, J. Phys. Chem. C **123**, 14734 (2019).

[17] S. A. Sato, Y. Shinohara, T. Otobe, and K. Yabana, Phys. Rev. B **90**, 174303 (2014).

[18] N. Tancogne-Dejean, O. Mücke, F. Kärtner, and A. Rubio, Nat. Commun. **8**, 745 (2017).

[19] P. D. Pemmaraju, F. D. Vila, J. J. Kas, S. A. Sato, J. J. Rehr, and K. Yabana, Comput. Phys. Commun. **226**, 30 (2018).

[20] S. A. Sato, K. Yabana, Y. Shinohara, T. Otobe, and G. F. Bertsch, Phys. Rev. B **89**, 064304 (2014).

[21] A. Guandalini, C. Cocchi, S. Pittalis, A. Ruini, and C. A. Rozzi, Phys. Chem. Chem. Phys. **23**, 10059 (2021).

[22] N. Schlünzen, K. Balzer, M. Bonitz, L. Deuchler, and E. Pehlke, Contrib. Plasma Phys. **59**, e201800184 (2019).

[23] L. Deuchler and E. Pehlke, Phys. Rev. B **102**, 235421 (2020).

[24] A. Kononov and A. Schleife, Phys. Rev. B **102**, 165401 (2020).

[25] K. Wu, H. Zhu, Z. Liu, W. Rodríguez-Córdoba, and T. Lian, J. Am. Chem. Soc. **134**, 10337 (2012).

[26] A. V. Akimov, A. J. Neukirch, and O. V. Prezhdo, Chem. Rev. **113**, 4496 (2013).

[27] D. Rudolf, C. La-O-Vorakiat, M. Battiato, R. Adam, J. M. Shaw, E. Turgut, P. Maldonado, S. Mathias, P. Grychtol, H. T. Nembach, T. J. Silva, M. Aeschlimann, H. C. Kapteyn, M. M. Murnane, C. M. Schneider, and P. M. Oppeneer, Nat. Commun. **3**, 1037 (2012).

[28] V. Cardin, T. Balciunas, K. Légaré, A. Baltuska, H. Ibrahim, E. Jal, B. Vodungbo, N. Jaouen, C. Varin, J. Lüning, and F. Légaré, Phys. Rev. B **101**, 054430 (2020).

[29] J. K. Dewhurst, P. Elliott, S. Shallcross, E. K. Gross, and S. Sharma, Nano Lett. **18**, 1842 (2018).

[30] J. Chen, U. Bovensiepen, A. Eschenlohr, T. Müller, P. Elliott, E. K. U. Gross, J. K. Dewhurst, and S. Sharma, Phys. Rev. Lett. **122**, 067202 (2019).

[31] K. Wu, J. Chen, J. R. McBride, and T. Lian, Science **349**, 632 (2015).

[32] R. Long and O. V. Prezhdo, J. Am. Chem. Soc. **136**, 4343 (2014).

[33] J. Zhang, M. Guan, J. Lischner, S. Meng, and O. V. Prezhdo, Nano Lett. **19**, 3187 (2019).

[34] K. Iida and M. Noda, npj Comput. Mater. **6**, 5 (2020).

[35] J. A. Tomko, E. L. Runnerstrom, Y.-S. Wang, W. Chu, J. R. Nolen, D. H. Olson, K. P. Kelley, A. Cleri, J. Nordlander, J. D. Caldwell, O. V. Prezhdo, J.-P. Maria, and P. E. Hopkins, Nat. Nanotechnol. **16**, 47 (2021).

[36] N. Rothenbach, M. E. Gruner, K. Ollefs, C. Schmitz-Antoniak, S. Salamon, P. Zhou, R. Li, M. Mo, S. Park, X. Shen, S. Weathersby, J. Yang, X. J. Wang, R. Pentcheva, H. Wende, U. Bovensiepen, K. Sokolowski-Tinten, and A. Eschenlohr, Phys. Rev. B **100**, 174301 (2019).

[37] L. Schumacher, J. Jose, D. Janoschka, P. Dreher, T. J. Davis, M. Ligges, R. Li, M. Mo, S. Park, X. Shen, S. Weathersby, J. Yang, X. Wang, F. Meyer zu Heringdorf, K. Sokolowski-Tinten, and S. Schlücker, J. Phys. Chem. C **123**, 13181 (2019).

[38] Y. Beyazit, J. Beckord, P. Zhou, J. P. Meyburg, F. Kühne, D. Diesing, M. Ligges, and U. Bovensiepen, Phys. Rev. Lett. **125**, 076803 (2020).

[39] I. I. Oleinik, E. Y. Tsymbal, and D. G. Pettifor, Phys. Rev. B **62**, 3952 (2000).

[40] W. H. Butler, X.-G. Zhang, T. C. Schulthess, and J. M. MacLaren, Phys. Rev. B **63**, 054416 (2001).

[41] B. Abedi Ravan, A. Shokri, and A. Yazdani, Solid State Commun. **150**, 214 (2010).

[42] M. E. Gruner and R. Pentcheva, Phys. Rev. B **99**, 195104 (2019).

[43] J. Mathon and A. Umerski, Phys. Rev. B **63**, 220403(R) (2001).

[44] C. Tiusan, J. Faure-Vincent, C. Bellouard, M. Hehn, E. Jouguelet, and A. Schuhl, Phys. Rev. Lett. **93**, 106602 (2004).

[45] D. Waldron, V. Timoshevskii, Y. Hu, K. Xia, and H. Guo, Phys. Rev. Lett. **97**, 226802 (2006).

[46] K. D. Belashchenko, J. Velev, and E. Y. Tsymbal, Phys. Rev. B **72**, 140404(R) (2005).

[47] C. Heiliger, P. Zahn, B. Y. Yavorsky, and I. Mertig, Phys. Rev. B **77**, 224407 (2008).

[48] J. Peralta-Ramos, A. M. Llois, I. Rungger, and S. Sanvito, Phys. Rev. B **78**, 024430 (2008).

[49] I. Rungger, O. Mryasov, and S. Sanvito, Phys. Rev. B **79**, 094414 (2009).

[50] X. Feng, O. Bengone, M. Alouani, S. Lebègue, I. Rungger, and S. Sanvito, Phys. Rev. B **79**, 174414 (2009).

[51] B. Eggert, M. E. Gruner, K. Ollefs, E. Schuster, N. Rothenbach, M. Y. Hu, J. Zhao, T. S. Toellner, W. Sturhahn, R. Pentcheva, B. R. Cuenya, E. E. Alp, H. Wende, and W. Keune, Phys. Rev. Materials **4**, 044402 (2020).

[52] N. Rothenbach, M. E. Gruner, K. Ollefs, C. Schmitz-Antoniak, S. Salamon, P. Zhou, R. Li, M. Mo, S. Park, X. Shen *et al.*, Phys. Rev. B **104**, 144302 (2021).

[53] T. Kaneko and T. Kanomata, *Landolt-Börnstein - Group IV Physical Chemistry 22A: Magnetic Properties of d-elements, Alloys and Compounds under Pressure* (Springer, Berlin, 2014).

[54] D. Roessler and W. Walker, Phys. Rev. **159**, 733 (1967).

[55] R. Whited, C. J. Flaten, and W. Walker, Solid State Commun. **13**, 1903 (1973).

[56] N.-P. Wang, M. Rohlfing, P. Krüger, and J. Pollmann, Appl. Phys. A: Mater. Sci. Process. **78**, 213 (2004).

[57] A. Schleife, F. Fuchs, J. Furthmüller, and F. Bechstedt, Phys. Rev. B **73**, 245212 (2006).

[58] M. Shishkin and G. Kresse, Phys. Rev. B **75**, 235102 (2007).

[59] B. Nourozi, A. Aminian, N. Fili, Y. Zangeneh, A. Boochani, and P. Darabi, Results Phys. **12**, 2038 (2019).

[60] M. Shishkin, M. Marsman, and G. Kresse, Phys. Rev. Lett. **99**, 246403 (2007).

[61] A. Schleife, C. Rödl, F. Fuchs, J. Furthmüller, and F. Bechstedt, Phys. Rev. B **80**, 035112 (2009).

[62] V. Begum, M. E. Gruner, C. Vorwerk, C. Draxl, and R. Pentcheva, Phys. Rev. B **103**, 195128 (2021).

[63] K. Dewhurst, S. Sharma *et al.*, The ELK code, version 6.2.8, http://elk.sourceforge.net/ (2019).

[64] J. P. Perdew and Y. Wang, Phys. Rev. B **45**, 13244 (1992).

[65] G. Kresse and J. Furthmüller, Phys. Rev. B **54**, 11169 (1996).

[66] G. Kresse and D. Joubert, Phys. Rev. B **59**, 1758 (1999).

[67] J. P. Perdew, K. Burke, and M. Ernzerhof, Phys. Rev. Lett. **77**, 3865 (1996).

[68] K. Krieger, J. Dewhurst, P. Elliott, S. Sharma, and E. Gross, J. Chem. Theory Comput. **11**, 4870 (2015).

[69] P. Elliott, T. Müller, J. Dewhurst, S. Sharma, and E. Gross, Sci. Rep. **6**, 38911 (2016).

[70] P. Elliott, K. Krieger, J. Dewhurst, S. Sharma, and E. Gross, New J. Phys. **18**, 013014 (2016).

[71] J. Dewhurst, K. Krieger, S. Sharma, and E. K. Gross, Comput. Phys. Commun. **209**, 92 (2016).

[72] U. Bierbrauer, S. T. Weber, D. Schummer, M. Barkowski, A.-K. Mahro, S. Mathias, H. C. Schneider, B. Stadtmüller, M. Aeschlimann, and B. Rethfeld, J. Phys.: Condens. Matter **29**, 244002 (2017).

[73] A. Eschenlohr, L. Persichetti, T. Kachel, M. Gabureac, P. Gambardella, and C. Stamm, J. Phys.: Condens. Matter **29**, 384002 (2017).

[74] See Supplemental Material at http://link.aps.org/supplemental/10.1103/PhysRevB.105.245103 for additional information concerning the impact of SOI on the time-dependent excitations, laser-induced excitations in MgO bulk, and the amplitude dependence of the transient excitation pattern.